A Generic Approach for Permittivity Measurement of Dielectric Materials Using a Discontinuity in a Rectangular Waveguide or a Microstrip Line

Jawad Abdulnour, Cevdet Akyel, *Member, IEEE,* and Ke Wu, *Senior Member, IEEE*

***Abstract*—A generic approach is proposed to accurately measure microwave and millimeter-wave properties of dielectric materials. This novel technique first determines the scattering parameters of a discontinuity containing a material having a wide range of complex dielectric permittivity ε that is known *a priori* (the direct problem). The discontinuity is embedded in a rectangular waveguide or a microstrip line. A unified theory, which is essentially based on a combination of the boundary integral equation technique with a modal expansion approach, is presented to tackle the direct problem. A class of generic diagrams are obtained for interrelating the dielectric permittivity ε to its S-parameters, and a simple analytical expression is deduced to solve the inverse problem. The proposed analytical formulation is easy to use and much more rapid than its iterative counterparts. It demonstrates a completely new and efficient strategy for accurate complex dielectric measurements.**

I. Introduction

THE knowledge of complex dielectric properties of materials is very important in studying the absorption of electromagnetic energy. A number of techniques are available for determining the complex dielectric parameters [1]–[3]. Each technique has its distinct advantages and drawbacks.

One of the most accurate techniques for determining dielectric parameters at high frequencies is the use of a resonant cavity having an extremely high quality factor [4], [5]. The disadvantage of this technique is that it is narrowband. With the advanced development of automatic network analyzers, a number of wideband techniques have been proposed [6]–[9]. These techniques are essentially based on measuring the scattering S-parameters of a discontinuity embedded in a transmission line. Weir [6] has presented an approach to directly determining the dielectric properties from a measurement of the S-parameters of a TEM-mode line. In this approach that was adopted by Barry [8] for a microstrip line, the dielectric under test is required to take up the entire discontinuity region. With this technique, a bad contact may result in up to a 40% measurement error for materials with a relatively high dielectric permittivity [9], [10]. In addition, there may be undesirable resonance phenomena and multiple solutions that preclude obtaining accurate results.

A coaxial line discontinuity that allows wideband measurements to be made has been used by Belhadj-Tahar *et al.* [9], who proposed an iterative technique. This technique was derived from the gradient method for calculating the permittivity ε from the S-parameters S_{11} and S_{21} (the inverse problem). For materials with a conductivity higher than 100 S/m at frequencies beyond 100 MHz, however, this approach is no longer valid because multiple solutions exist [11].

The method that uses a cylindrical post in a rectangular waveguide has been examined by several authors [12]–[14]. The advantage of this technique is that these samples are easily fabricated and handled. Moreover, the resonance and multiple-solution problems can be easily controlled by reducing the cylinder dimensions. The frequency bandwidth is limited by the cut-off frequency of the fundamental mode and that of the first higher-order mode. This limitation can be overcome through the use of multiple guides (it is possible to cover easily the bandwidth between 8 and 26 GHz with three rectangular guides, for instance). In a rigorous electromagnetic modeling and analysis of a discontinuity along transmission lines (including rectangular waveguides), it is necessary to take into account the effect of higher-order modes. In parallel, it may be difficult to obtain an analytical solution that allows dielectric permittivities to be determined from the scattering S-parameters (the inverse problem). Usually, there are two types of methods: the iterative methods and the graphical methods. The former demands a significant amount of CPU time and may fail to converge if the initial guesses fall outside of a reasonable range of solutions, while the latter technique requires a considerable number of curves per frequency to achieve reasonable precision.

In this paper, a unified method is proposed for calculating the scattering S-parameters, knowing *a priori* the permittivity of a dielectric post embedded in a rectangular waveguide or a microstrip line. By applying this method, a class of generic diagrams are established, showing characteristics of the S-parameters as functions of ε. Based on these diagrams, a simple analytical equation is proposed for directly determining an unknown dielectric permittivity from the parameters S_{11} and S_{21}. The proposed theories for the direct and inverse problems are also verified and confirmed by our measurements for various samples.

Manuscript received June 27, 1994; revised September 26, 1994. This work was supported by the Natural Sciences and Engineering Research Council (NSERC) of Canada.

The authors are with the Groupe de Recherches Avancées en Microondes et en Électronique Spatiale, Dept. de génie électrique et de Génie Informatique, École Polytechnique, Montréal H3C 3A7, Canada .

IEEE Log Number 9410327.

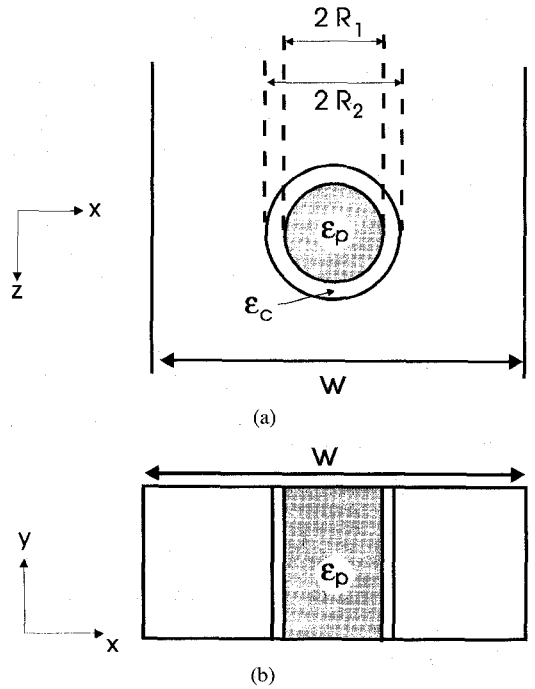

Fig. 1. A rectangular waveguide with a dielectric cylinder containing a sample under test. (a) View from the top. (b) View from the side.

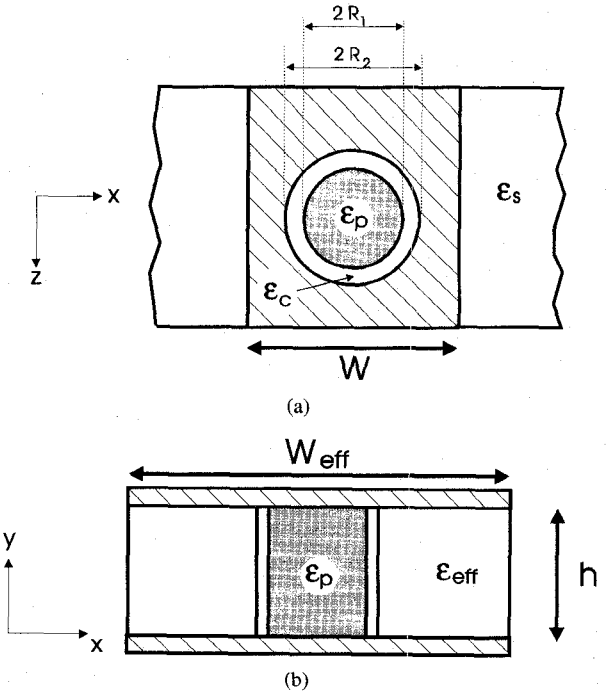

Fig. 2. A microstrip line with a dielectric cylinder containing a sample under test. (a) View from the top with physical parameters. (b) View from the side with effective parameters.

II. Direct Problem

A. Theoretical Formulation

The cells to be studied are shown in Figs. 1 and 2 with the longitudinal direction being z and the transverse section x–y. The dielectric material to be analyzed may be a cylindrical homogeneous dielectric or a liquid confined in a dielectric tube. The geometry is divided into three regions: I and II represent the uniform portions of the line and one discontinuity region is denoted as Ω in Fig. 3. The boundary Γ of the discontinuity region is divided into four pieces: Γ_1 for the interface with the region I, Γ_2 for the interface with the region II, Γ_3 for an electric wall (rectangular waveguide) or a magnetic wall (microstrip line), and Γ_4 for the boundary of the dielectric cylinder.

The electric field E_y within the discontinuity region Ω satisfies Helmholtz equation with associated boundary conditions. Using the fundamental solution and Green's identity [15], [16] leads to

$$\frac{E_y(\vec{r}_p)}{2} = \int_\Gamma \left[\frac{\partial E_y(\vec{r})}{\partial n} u_p^* - E_y(\vec{r}) q_p^*\right] d\Gamma \tag{1}$$

in which n is the normal unit vector on the boundary Γ, u^*, and q^* denote the Green's function for Helmholtz equation and its normal derivative. They have been given in [15], [16].

B. Modal Expansion

The fundamental mode is assumed to be incident into the region I (see Fig. 3) and its magnitude is normalized; the corresponding field and its normal derivative on the interface Γ_1 can be written as in the following:

$$E_y = \varphi_1 e^{\gamma_1 l_1} + \sum_{m=1}^{N_1} R_m \varphi_m e^{-\gamma_m l_1} \tag{2}$$

$$\frac{\partial E_y}{\partial n} = -\frac{\partial E_y}{\partial z} = \gamma_1 \varphi_1 e^{\gamma_1 l_1} - \sum_{m=1}^{N_1} R_m \gamma_m \varphi_m e^{-\gamma_m l_1}. \tag{3}$$

On the interface Γ_2,

$$E_y = \sum_{m=1}^{N_2} T_m \varphi_m e^{-\gamma_m l_2} \tag{4}$$

$$\frac{\partial E_y}{\partial n} = -\frac{\partial E_y}{\partial z} = -\sum_{m=1}^{N_2} T_m \gamma_m \varphi_m e^{-\gamma_m l_2} \tag{5}$$

where R_m and T_m are unknown coefficients that represent the magnitudes of the reflected and the transmitted modes, respectively. Here $l_1 + l_2$ is the length of the discontinuity region along z-direction. This implies that the reference plans are placed at $z = -l_1$ and $z = l_2$. N_1 and N_2 are the numbers of the reflected and transmitted modes, respectively. N_1 and N_2 should be infinite theoretically. In practice, a dozen of modes turn out to be largely sufficient for a good convergence. In the case of a rectangular waveguide, the modal functions can be written as

$$\varphi_m = \sin\left(\frac{m\pi}{w} x\right) \tag{6}$$

$$\gamma_m = \sqrt{\left(\frac{m\pi}{w}\right)^2 - \omega^2 \mu_0 \varepsilon_0}. \tag{7}$$

In the case of a microstrip line, the modal functions become

$$\varphi_m = \cos\left(\frac{(m-1)\pi}{w_{eff}} x\right) \tag{8}$$

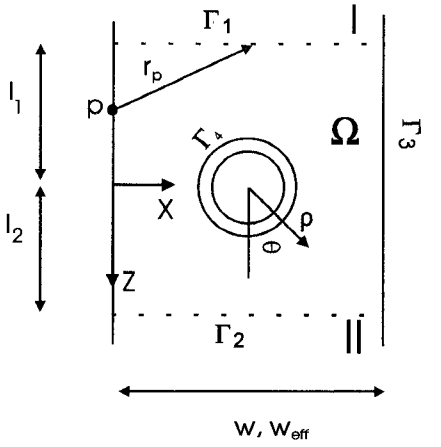

Fig. 3. The discontinuity region.

$$\gamma_m = \sqrt{\left(\frac{(m-1)\pi}{w_{eff}}\right)^2 - \omega^2 \mu_0 \varepsilon_0 \varepsilon_{eff}} \tag{9}$$

in which the well-known concept of the planar waveguide model is used. In this model, the microstrip width w and the substrate permittivity ε_s are replaced by their effective values w_{eff} and ε_{eff}. There exist several techniques for calculating the dynamic effective values considering the dispersion effect [17], [18]. In this work, the analytical formulation proposed by Kobayashi is used. This formula yields a precision on the order of 1% for $0.1 < w/h < 10$ and $1 < \varepsilon_s < 100$, where h is the substrate thickness. It should be noted that the presence of a dielectric post affects the field distribution inside the region Ω, and therefore the effective values have to be modified accordingly in proximity to the post. The experimental values given by Finch and Alexopoulos [19] demonstrate that this perturbation does not much affect the results. Hence this factor is ignored for the moment, and its influence can be eliminated by a simple calibration.

C. Dielectric Cylinder

Based on a system of polar coordinate ρ, θ, the origin of which coincides with the center of the cylinder (see Fig. 3), the electric field on the boundary Γ_4 can be expressed in terms of unknown coefficients A_n, such that

$$E_y = \sum_{n=-\infty}^{\infty} A_n Z_n e^{-jn\theta} \tag{10}$$

in which

$$Z_n = \left[\frac{f_n}{g_n} J_n(K_2 R_2) + Y_n(K_2 R_2)\right]$$

where

$$f_n = \frac{K_2}{K_1} \frac{Y_n'(K_2 R_1)}{J_n'(K_1 R_1)} - \frac{Y_n(K_2 R_1)}{J_n(K_1 R_1)}$$

and

$$g_n = \frac{J_n(K_2 R_1)}{J_n(K_1 R_1)} - \frac{K_2}{K_1} \frac{J_n'(K_2 R_1)}{J_n'(K_1 R_1)}.$$

In these equations, J_n and Y_n are Bessel and Neumann functions, respectively. $K_1 = \omega^2 \mu_0 \varepsilon_0 \varepsilon_p$ and $K_2 = \omega^2 \mu_0 \varepsilon_0 \varepsilon_c$ are the propagation constants in the sample and the tube surrounding the sample, respectively.

The infinite series in (10) can be truncated into a finite number $N_4 = 2N' - 1$, which allows one to write the following equations:

$$E_y = \sum_{n=1}^{N_4} P_n \psi_n, \tag{11}$$

with

$$\psi_n = Z_{n-1} \cos[(n-1)\theta] \qquad \text{for } n \le N'$$
$$\psi_n = Z_{n-N'-1} \sin[(n-N'-1)\theta] \qquad \text{for } n > N'.$$

The normal derivative of (11) is

$$\frac{\partial E_y}{\partial n} = -\frac{\partial E_y}{\partial \rho} = -\sum_{n=1}^{N} P_n \psi_n' \tag{12}$$

where ψ_n' is the derivative of ψ_n with respect to ρ

D. Matrix Formulation

To begin with, substituting (2)–(5) and (11) into (1), we let the pointer p run N_1 points over the trajectory Γ_1, N_2 points over Γ_2 and N_4 points over Γ_4. The magnetic or electric walls are subdivided into N_3 elements for which the boundary element technique [16], [20] is applied. It is easy to obtain the following linear system:

$$\begin{bmatrix} [A^{11}] & [A^{12}] & [A^{13}] & [A^{14}] \\ [A^{21}] & [A^{22}] & [A^{23}] & [A^{24}] \\ [A^{31}] & [A^{32}] & [A^{33}] & [A^{34}] \\ [A^{41}] & [A^{42}] & [A^{43}] & [A^{44}] \end{bmatrix} \begin{bmatrix} \{R\}_{\Gamma_1} \\ \{T\}_{\Gamma_2} \\ \{U\}_{\Gamma_3} \\ \{P\}_{\Gamma_4} \end{bmatrix} = \begin{bmatrix} \{V^1\} \\ \{V^2\} \\ \{V^3\} \\ \{V^4\} \end{bmatrix}. \tag{13}$$

The submatrices $[A^{\alpha\beta}]\,(\alpha, \beta = 1, 2, 3, 4)$ have dimensions of $N_\alpha \times N_\beta$, and the elements of these matrices are given by

$$A_{ij}^{\alpha\beta} = \left\{\tfrac{1}{2}\varphi_j(x_i)\delta_{\alpha\beta} + \int_0^w \varphi_j(q_i^* + \gamma_j u_i^*)\, dx\right\} e^{-\gamma_j l_\beta} \qquad (\beta = 1, 2) \tag{14}$$

and

$$A_{ij}^{\alpha 4} = \tfrac{1}{2}\psi_j(\theta_j)\delta_{\alpha 4} + \int_0^{2\pi} (\psi_j q_i^* + \psi_j' u_i^*)\, d\theta. \tag{15}$$

The elements of the submatrices $[A^{\alpha 3}]$ depend on the choice of the boundary elements on the electric or magnetic wall. In this work, the constant elements are chosen [20] (the field or its derivative is supposed to be constant over the elements). In the case of a rectangular waveguide (electric wall), the vector $\{\mathbf{U}\}_{\Gamma_3}$ consists of normal derivatives of the field on the elements over Γ_3 and

$$A_{ij}^{\alpha 3} = -\int_{el_j} u_i^*\, d\Gamma. \tag{16}$$

In the case of a microstrip line (magnetic wall), the vector $\{\mathbf{U}\}_{\Gamma_3}$ consists of the field values on the elements and

$$A_{ij}^{\alpha 3} = \int_{el_j} q_i^*\, d\Gamma. \tag{17}$$

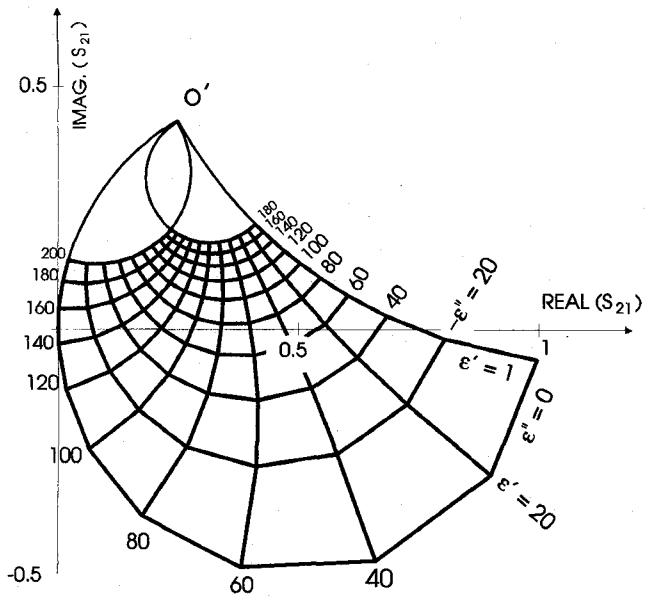

Fig. 4. Diagram illustrating the variation of complex permittivity versus scattering parameters in the complex plane at 8 GHz for a rectangular waveguide. A Pyrex cylinder having $\varepsilon_c = 4.5, R_1 = 0.54$ mm, and $R_2 = 0.866$ mm was used in the calculation.

The elements of the vectors $\{\mathbf{V}^\alpha\}$ are given by

$$\mathbf{V}_i^\alpha = -\left[\frac{1}{2}\,\varphi_1(x_i)\delta_{\alpha 1} + \int_0^w \varphi_1(q_i^* - \gamma_1 u_i^*)\,dx\right] e^{\gamma_1 l_1}. \tag{18}$$

The vectors $\{\mathbf{R}\}_{\Gamma_1}$ and $\{\mathbf{T}\}_{\Gamma_2}$ are composed of complex magnitudes of the reflected modes R_m and transmitted modes T_m at the interfaces Γ_1 and Γ_2, respectively. The vector $\{\mathbf{P}\}_{\Gamma_4}$ consists of the unknown coefficients P_n, which appear in (11). Since the magnitude of the incident mode is normalized, the solution of (13) yields the S-parameters directly, or more precisely, $S_{11} = R_1$ and $S_{12} = T_1$.

III. Inverse Problem

One of the greatest difficulties encountered in the dielectric measurement using a discontinuity in a transmission line is to solve inverse problem. This is equivalent to saying that a dielectric permittivity ε is to be calculated from knowing the S-parameters. So far, a number of iterative approaches have been proposed [9], and the main problems with this type of techniques lie in a relatively long CPU time and various convergence difficulties. The graphic technique based on solution diagrams similar to Fig. 4 is proposed as an alternative for solving the inverse problem. These diagrams permit one to localize the dielectric permittivity to be determined by knowing the real and imaginary parts of S_{11} or S_{21}. In order to achieve an acceptable accuracy with this technique, a considerable number of curves per frequency should be plotted, which is not particularly practical. In this paper, a simple analytical yet accurate expression is proposed to calculate ε directly from S_{11} or S_{21}.

In analyzing Fig. 4, it is found that the curves $\varepsilon' = \text{cst.}$ and $\varepsilon'' = \text{cst.}$ form a number of circular arcs that pass through the same point o' whose coordinates (xo', yo') correspond to the transmission coefficient of a conducting cylinder with a radius of R_1. Fig. 5 shows locations of the geometrical centers of all circular arcs. The points A_a and B_b are the centers of the arcs for $\varepsilon = a$ and $\varepsilon = b$. The coordinates of these points in $(x'o'y')$ axes system are $(x'_{Aa}, 0)$ and $(0, y'_{Bb})$.

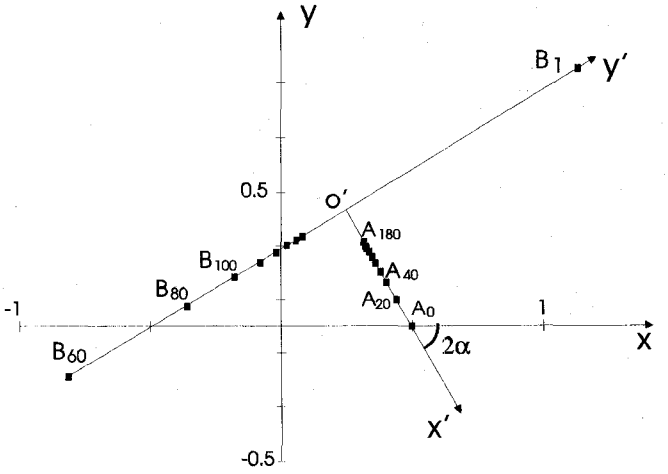

Fig. 5. Locations of geometrical centers of the circular arc $e' = \text{const.}$ and $e'' = \text{const.}$

Figs. 6 and 7 demonstrate variations of $1/x'_{Aa}$ against ε'' and $1/y'_{Bb}$ versus ε'. It is surprisingly found, regardless of frequency and cylindrical radius, that this variation is always linear and the two curves have an inverse sign. In addition, $x'_{A0} = 0.5$ is obtained for $\varepsilon'' = 0$, which allows one to derive a generic expression, such that

$$\varepsilon' = C\left[\frac{2y'_p}{y'^2_p + x'^2_p} - tg(\alpha - \beta)\right] + 1 \tag{19a}$$

and

$$\varepsilon'' = -C\left[\frac{2x'_p}{y'^2_p + x'^2_p} - 1\right] \tag{19b}$$

where

$$y'_p = (y_p - y_{o'})\cos(2\alpha) - (x_p - x_{o'})\sin(2\alpha)$$
$$x'_p = (x_p - x_{o'})\cos(2\alpha) + (y_p - y_{o'})\sin(2\alpha)$$

and

$$\alpha = \text{atan}\left(\frac{x_{o'}}{y_{o'}}\right)$$
$$\beta = \text{atan}\left(\frac{y_{p0}}{x_{p0}}\right).$$

In these equations, $S_{21}^v = x_{p0} + jy_{p0}$ is the transmission coefficient for the empty cylinder (without sample) and $S_{21} = x_p + jy_p$ is for the cylinder filled up with sample. These two parameters are measurable. $x_{o'}, y_{o'}$ and C can therefore be calculated easily by solving the direct problem.

In the case of a microstrip line, diagrams similar to these shown in Fig. 4 can be obtained, and the same expressions as (19) can be derived by the same procedure. As it has been mentioned above, the presence of a post in the case of a microstrip line affects the effective parameters of the line in the planar waveguide model, and subsequently $x_{o'}, y_{o'}$, and C.

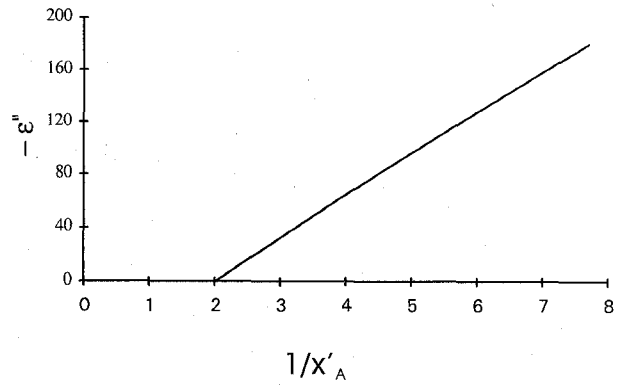

Fig. 6. Variation of $1/x'_A$ as a function of the imaginary part of the complex permittivity.

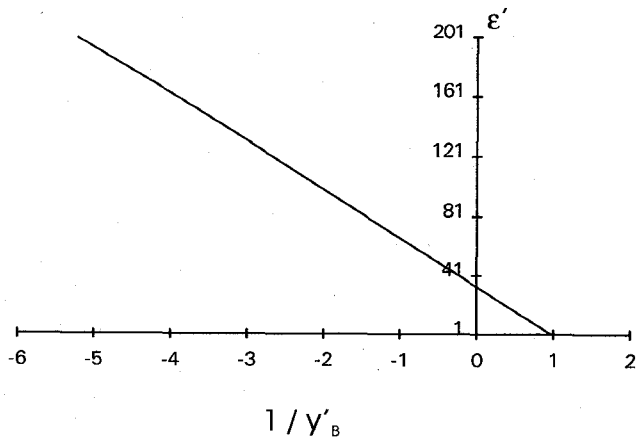

Fig. 7. Variation of $1/y'_B$ as a function of the real part of the complex permittivity.

This problem can be remedied by measuring experimentally $S_{21}^c = x_{o'} + jy_{o'}$, representing the transmission coefficient for a metallic post that shares the same dimensions as the sample. The coefficient C can be determined by a calibration procedure. This is easily done by using a dielectric material as the sample whose dielectric permittivity is known.

The S-parameters considered above are determined at the reference plane that is located at the cylinder center. Experimentally speaking, the calibration is usually made at reference plans $z = -l_1$ and $z = l_2$. To return the reference plane to the cylinder center, the transmission coefficients measured at $z = -l_1$ and $z = l_2$ are divided by S_{21}^0 that corresponds to the counterpart measured at $z = l_2$ for the through line with a length equal to $l_1 + l_2$ under the absence of the cylinder and sample. The procedure for moving the reference plane instead of the sample provides an additional advantage that a high-precision measurement of the lengths l_1 and l_2 can be effectively avoided, and subsequently a major source of error is eliminated. In the absence of a dielectric cylinder surrounding the sample, S_{21}^v is simply equal to 1.

IV. Results and Discussion

To confirm the validity of (19), results are directly calculated for a number of values of ε. The obtained parameters S_{21} are used in (19) to verify whether the same values of *a priori* known ε can be obtained with a precision better than 1%. It is found that, in the case of considering a rectangular waveguide with $1.2 \times f_c^{\mathrm{TE}_{10}} < f < 1.8 \times f_c^{\mathrm{TE}_{10}}$, the proposed (19) is always valid for whatever value of $R_1 \leq 0.1 \times w$. In the case of a microstrip line for $f < 0.5 \times f_{c2}$ in which f_{c2} is the cut-off frequency of the first higher-order mode, (19) is once again shown to be valid for whatever value as long as $R_1 \leq 0.3 \times w$. This allows one to use this formula over a sufficiently large bandwidth. In the following examples, a microstrip line with $\varepsilon_s = 2.18$,$w = 0.482$ cm, and $h = 0.157$ cm is used to cover the frequency bands L, S and C (1–7 GHz). For X, Ku, and K bands (8–26 GHz), three rectangular waveguides (WR-90, WR-62, and WR-42) are used. The S-parameters are measured with a HP8510 network analyzer using a TRL calibration procedure.

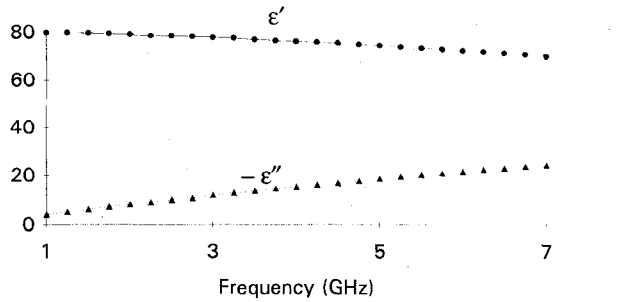

Fig. 8. The measured and extracted complex permittivity of water in a cylindrical cell embedded in a microstrip line at the room temperature between 1 and 7 GHz.

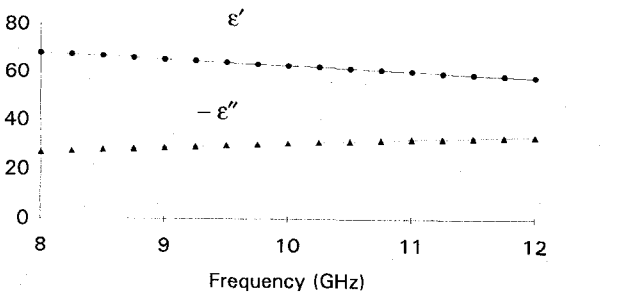

Fig. 9. The measured and extracted complex permittivity of water in the rectangular waveguide WR-90 at the room temperature between 8 and 12 GHz.

Figs. 8 and 9 show the measured complex permittivity of water at the room temperature. The microstrip line technique was used for the frequency range of 1–7 GHz (Fig. 8) with a cylinder radius of 0.12 cm. A rectangular waveguide WR-90 was used to cover the frequency range between 8 and 12 GHz as shown in Fig. 9. The water was contained in the waveguide with a Pyrex tube having $R_1 = 0.054$ cm and $R_2 = 0.086$ cm. The two measurements made using different techniques seem to be consistent because they connect smoothly when extrapolated in the range 7–8 GHz. In addition, the results agree well with those given by National Bureau of Standard circular 589, which are $\varepsilon' = 77.8$ and $\varepsilon'' = 13.9$ at the room temperature of 20°C and a frequency of 3.25 GHz.

The measured complex permittivities of two known materials (Teflon and Plexiglas) are shown in the Table I. The samples used here were in the form of rods with a radii of

TABLE I
THE MEASURED AND EXTRACTED COMPLEX PERMITTIVITY OF TEFLON AND PLEXIGLASS AT SEVERAL FREQUENCIES USING THE TECHNIQUE OF RECTANGULAR WAVEGUIDES

	Teflon		plexiglass	
Freq. (GHz)	ε'	$-\varepsilon''$	ε'	$-\varepsilon''$
8	2.05	0.006	2.61	0.01
10	2.04	0.007	2.59	0.008
12	2.05	0.006	2.61	0.009
14	2.03	0.004	2.6	0.007
16	2.03	0.005	2.58	0.007
18	2.05	0.003	2.6	0.01
20	2.04	0.006	2.6	0.007
22	2.03	0.003	2.59	0.008
24	2.02	0.004	2.59	0.006
26	2.02	0.003	2.58	0.006

TABLE II
THE MEASURED AND EXTRACTED COMPLEX PERMITTIVITY OF A CLASS OF POLYMER MATERIALS WITH AND WITHOUT DOPING AT 15 GHz USING THE RECTANGULAR WAVEGUIDE WR-62

	Base		Doped	
	ε'	$-\varepsilon''$	ε'	$-\varepsilon''$
PNEtA	3.14	0.06	4	0.13
PNPeA	3	0.04	3.4	0.1
PNPrA	3.2	0.05	5.3	0.2
PNMeA	3.3	0.05	6.1	0.43
PNBuA	3.1	0.04	3.4	0.06
PNDoA	2.3	0.01	2.3	0.02

$R = 0.95$ mm for WR-90 and $R = 0.47$ mm for WR-62 and WR-42. The measured results are in good agreement with published data.

Our approach was applied to studying characteristics of conducting polymer materials at microwave frequencies. It is known that electrical properties such as the conductivity and permittivity of certain polymers change if they are subjected to an acid process (protonation) [11], [21]. The permittivity and conductivity may be controlled by changing the degree of doping acidity. This renders these materials very interesting for the purpose of absorbing electromagnetic energy.

Shown in the Table II are the measured complex permittivities of certain polymer poly(N-alkylanilines)-based materials at 15 GHz and the room temperature. The samples were compressed powders made with a pressure of 1.8 tons/cm^2 in the form of cylindrical capsules with radius of 1.5 mm, 0.6 mm, and a height that varies from 1–2 mm. The capsules were then put into a Teflon envelop with a thickness of 0.2 mm in order to obtain posts having the same height as the waveguides. The doping was achieved by processing the polymers in a solution of an acid called tetrafluoborat $H(FB)_4$ 0–2 pH. It was found that there is a slight increase in the complex permittivity when the polymer is doped. However, such a small incremental increase is not sufficient for considering these products as conducting polymers.

One of the most promising polymers is the polyaniline PANI, which is stable at the room temperature and whose conductivity can be controlled between 10^{-8} and 500 S/m [11]. The doped PANI-based samples were measured in the three rectangular waveguides. The PANI based polymer without processing exhibits a complex permittivity of $\varepsilon = 4.2 - j0.01$, which remains nearly unchanged between 8 and 26 GHz. Fig. 10 shows the frequency-dependent complex permittivity over the frequency range of interest for a doped PANI material. For the imaginary part of the permittivity, the variation of log ε versus log f is quasilinear, and the results fall in the same order of values as those obtained by De Chanterac *et al.* [11] who have measured the PANI processed with a solution of acid called chlorhydrique HC1. Nevertheless, these authors have not shown any results for the real part of permittivity with pH = 0–2. This may be attributed to the limitation of their measurement range.

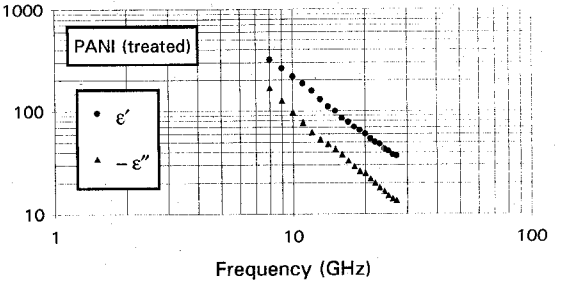

Fig. 10. Frequency-dependent complex permittivity of polyaniline processed with a very acid solution pH = 0–2.

V. CONCLUSION

A simple generic, yet accurate, approach is presented for determining the complex permittivity of dielectric materials based on a rectangular waveguide and microstrip line measurement technique. A unified theory that combines the boundary integral equation technique with the modal field expansion technique is proposed to calculate the scattering parameters by knowing *a priori* a set of permittivities (the direct problem). This method is used to generate a number of graphic diagrams showing variations of complex permittivity as functions of the scattering parameters in the complex plane. A very simple analytical expression is deduced from these diagrams to solve the inverse problem. This proposed formula, leading to very good results, is very easy to use and much faster than its iterative or its graphic counterparts. Some known materials are measured and analyzed to validate the proposed approach. Using the novel method, complex permittivity for a class of polymer materials with and without acid doping are determined.

REFERENCES

[1] C. G. Montgomery, *Technique of Microwave Measurements.* New York: McGraw-Hill, 1947.
[2] A. R. Von Hipple, Ed., *Dielectric Materials and Applications.* New York: Wiley, 1954.
[3] M. Sucher and J. Fox, *Handbook of Microwave Measurements,* 3rd ed. New York: Wiley, 1963.
[4] R. Dunsmuir and J. G. Powles, "A method for the measurement of the dielectric properties in the frequency range 600–3200 Mc/sec (50–9.4 cm)," *Philos. Mag.*, ser. 7, vol. 37, pp. 747–756, 1946.

[5] G. Birnbaum and J. Franeau, "Measurement of the dielectric constant and loss of solids and liquids by a cavity perturbation method," *J. Appl. Phys.,* vol. 20, pp. 817–818, 1949.
[6] W. B. Weir, "Automatic measurement of complex dielectric constant and permeability at microwave frequencies," *Proc. IEEE,* vol. 62, pp. 33–36, Jan. 1974.
[7] L. P. Ligthart, "A fast computational technique for accurate permittivity determination using transmission line methods," *IEEE Trans. Microwave Theory Tech.,* vol. MTT-31, pp. 249–254, Mar. 1983.
[8] W. Barry, "A broad-band, automated, stripline technique for the simultaneous measurement of complex permittivity and permeability," *IEEE Trans. Microwave Theory Tech.,* vol. MTT-34, pp. 80–84, Jan. 1986.
[9] N. Belhadj-Tahar, A. Fourrier-Lamer, and H. De Chanterac, "Broad-band simultaneous measurement of complex permittivity and permeability using a coaxial discontinuity," *IEEE Trans. Microwave Theory Tech.,* vol. MTT-38, pp. 1–7, Jan. 1990.
[10] K. E. Mattar, D. G. Watters, and M. E. Brodwin, "Influence of wall contacts on measured complex permittivity spectra at coaxial line frequencies," *IEEE Trans. Microwave Theory Tech.,* vol. MTT-39, pp. 532–537, Mar. 1991.
[11] H. De Chanterac, N. Belhadj-Tahar, and A. Fourrier-Lamer, "Electromagnetic absorption of polyanilines at microwave frequencies," *Synthetic Metals,* vol. 52, pp. 183–192, 1992.
[12] E. D. Nielsen, "Scattering by a cylindrical post of complex permittivity in a waveguide," *IEEE Trans. Microwave Theory Tech.,* vol. MTT-17, pp. 148–153, Mar. 1969.
[13] J. N. Sahalos and E. Vafiadis, "On the narrow-band microwave filter design using a dielectric rod," *IEEE Trans. Microwave Theory Tech.,* vol. MTT-33, pp. 1165–1171, Oct. 1985.
[14] J. Abdulnour and L. Marchildon, "Scattering by a dielectric obstacle in a rectangular waveguide," *IEEE Trans. Microwave Theory Tech.,* vol. MTT-41, pp. 1988–1994, Nov. 1993.
[15] M. Koshiba and M. Suzuki, "Application of the boundary-element method to waveguide discontinuities," *IEEE Trans. Microwave Theory Tech.,* vol. MTT-34, pp. 301–307, Feb. 1986.
[16] J. Abdulnour and L. Marchildon, "Boundary elements and analytic expansions applied to H-plane waveguide junctions," *IEEE Trans. Microwave Theory Tech.,* vol. MTT-42, June 1994.
[17] M. Kirschning and R. H. Jansen, "Accurate model for effective dielectric constant of microstrip with validity up to millimeter-wave frequencies," *Electron. Lett.,* vol. 18, pp. 272–273, 1982.
[18] M. Kobayashi, "A dispersion formula satisfying recent requirements in microstrip CAD," *IEEE Trans. Microwave Theory Tech.,* vol MTT-36, pp. 1246–1250, Aug. 1988.
[19] K. L. Finch and N. G. Alexopoulos, "Shunt posts in microstrip transmission lines," *IEEE Trans. Microwave Theory Tech.,* vol. MTT-38, pp. 1585–1594, Nov. 1990.
[20] C. A. Brebbia and S. Walker, *Boundary Element Techniques in Engineering.* London: Butterworths, 1980.
[21] J. Chevalier, J. Bergeron, and L. H Dao, "Synthesis, characterization, and properties of Poly(N-alkylanilines)," *Macromolecules,* vol. 25, no. 13, pp. 3325–3331, 1992.

Jawad Abdulnour was born in Cheikh-Taba, Lebanon, in 1960. He completed his undergraduate studies in physics at the Lebanese University in Beyrouth in 1982. He spent several years in France, and then went to the Université du Québec à Trois Rivières, where he received the M.Sc. degree in physics in 1989 and the Ph.D. degree in energy sciences in 1993.

He is currently working as a research associate at Ecole Polytechnique, Montréal.

Cevdet Akyel (S'74–M'79–S'80–M'80–M'88) was born in Samsun, Turkey, in 1945. He received the B.Sc. degree in electrical engineering from the Technical University of Istanbul in 1971. He then obtained the M.Sc.A. degree in microwave measurements and the Ph.D. degree in electrical engineering from Ecole Polytechnique, Universt é de Montréal, in 1975 and 1980, respectively.

He worked as a system engineer at the Northen Telecom Company, in Montréal, from 1974–1976. He held the position of NSERC research fellow at Ecole Polytechnique from 1980–1985, and since then has been teaching electrical engineering there.

Ke Wu (M'87–SM'92), for a photograph and biography, see p. 1114 of this TRANSACTIONS.